The Control and Mechanics of Human Movement Systems

Clyde F. Martin and Lawrence Schovanec [1]

1 Introduction

Issues that are central to the modeling and analysis of a human movement system include (1) musculotendon dynamics, (2) the kinetics and kinematics of the biomechanical system, and (3) the relationship between neurological control and the formulation of the system as an open or closed loop process. This paper will address these problems in the context of two particular movement systems. The first to be addressed is the human ocular system. Eye movement systems are ideal for studying human control of movement since they are of relatively low dimension and easier to control than other neuromuscular systems. By scrutinizing the trajectories of eye movements it is possible to infer the effects of motoneuronal activity, deduce the central nervous system's control strategy, and systematically observe the effects of perturbations in the controls. An application of the locomotory-control system will also be presented in this paper. In particular, a model of human gait is developed for the purpose of relating neural controls to the state of stress in a skeletal member. This is achieved by modeling the human body as an ensemble of articulating rigid-body segments controlled by a minimal muscle set. Neurological signals act as the input into the musculotendon dynamics and from the resulting muscular forces, the joint moments and resulting motion of the segmental model are derived. At fixed moments in the gait cycle, the joint torques and joint reaction forces are incorporated into an equilibrium analysis of the segmental elements, modeled as elastic bodies undergoing biaxial bending. Both movement systems that are discussed here emphasize a forward or direct dynamic approach that results in a natural flow of neural-to-muscular-to-movement events while utilizing physiologically realistic models of the musculotendon actuators that faithfully reproduce trajectories and muscle tension.

1.1 Inverse versus Forward Dynamics

If a movement system has n degrees of freedom, then the equations of motion governing the system can be written in the form

$$[M(\theta)]\ddot{\theta} = C(\theta, \dot{\theta}) + G(\theta) + F_m(\theta) \tag{1.1.1}$$

[1]This research was supported by NSF grants ECS-9720357, DMS-9628558 and Texas Advanced Research Program Grant No. 003644-123.

where $\theta, \dot{\theta}, \ddot{\theta}$ are $n \times 1$ vectors of displacement, velocity and acceleration, $[M(\theta)]$ is the $n \times n$ inertia matrix, $C(\theta, \dot{\theta})$ is an $n \times 1$ vector of coriolis and centrifugal terms, $G(\theta)$ is an $n \times 1$ vector of gravitational terms, and $F_m(\theta)$ is an $n \times 1$ vector of applied moments. There are are essentially two approaches to analyzing such a movement system.

Inverse dynamics is an approach that proceeds from known kinematic data and external forces and moments to arrive at expressions for the resultant forces and moments. For this method, motion acts as the input and torques are the output. This approach requires experimental and kinematic data and observed motions. If these variables are assumed to be known functions of time, (1.1.1) becomes an algebraic equation for $F_m(\theta)$. It is a difficult problem however, to determine the forces of the individual muscles that result in an applied moment since there are typically more unknown muscle forces than can be determined from mechanical relations alone. This is referred to as the *redundancy problem*. To address this problem the muscle set that contributes to a specific motion may be reduced by grouping muscles of similar function or by using EMG activity as a guide in determining which muscles were used during a specific movement [4, 20, 24]. If the problem is still indeterminate, a static optimization scheme is employed. For these types of optimization methods the selection of appropriate optimization criterion is somewhat arbitrary and the schemes do not take into account musculotendon dynamics [8, 26, 13]. Consequently, the static optimization approach often results in discontinuous muscle force histories [29]. Another limitation associated with the inverse method is that it is not predictive in nature in that one is limited to studying motion which is produced by monitored subjects.

In contrast, the forward or direct-dynamic approach provides the motion of the system over a given time period as a consequence of the applied forces and given initial conditions. Solution of the forward dynamics problem makes it possible to simulate and predict motion as a result of the forces that produce it. In a forward analysis the torques or the muscle forces that generate the moments are the inputs and the body motion is the output. This relationship is emphasized by writing equation (1.1.1) in the form

$$\ddot{\theta} = [M(\theta)]^{-1}(C(\theta, \dot{\theta}) + G(\theta) + F_m(\theta)).$$

Since neural input activates the muscles, i.e., the actuators of the system, the true input into the system is indeed neural input. Because controls for each muscle are needed, the redundancy problem reoccurs. In the forward approach, muscle dynamics are incorporated into the optimization techniques used to determine the controls. For instance, when human gait is to be simulated, the dynamic optimization methods employ cost functions that usually involve both a tracking error term and a term influencing the distribution of muscle force [9]. Once controls are achieved, the system of differential equations for the body segments and the muscle groups can be

integrated forward in time to obtain the motion trajectories. In this sense, a direct-dynamic analysis is self-validating in that the controls specified do indeed result in the observed motion.

A complete development of a direct dynamic model needs to include a representation of the musculotendon complex, anatomical geometry, and kinematic models and inertial characteristics of the underlying movement system. In the next section we provide an overview of musculotendon dynamics. In subsequent sections we utilize these dynamics in developing movement systems that describe ocular motion and human gait. Within the context of these specific applications we will present the relevant geometrical, kinematical, and inertial information.

2 Musculotendon Dynamics

2.1 Functional Properties

Muscles are the actuators of the neuro-musculo-skeletal control system that produce movement. In the analysis of a control system as complex as that governing movement it is essential to have a clear understanding of the physical nature of the actuators and a tractable mathematical representation of their dynamics. The muscle models utilized in this investigation are referred to as Hill-type models. A phemenological representation of the musculotendon complex as idealized mechanical objects is presented in Figure 1. This model has been shown to incorporate enough complexity while remaining computationally practical.

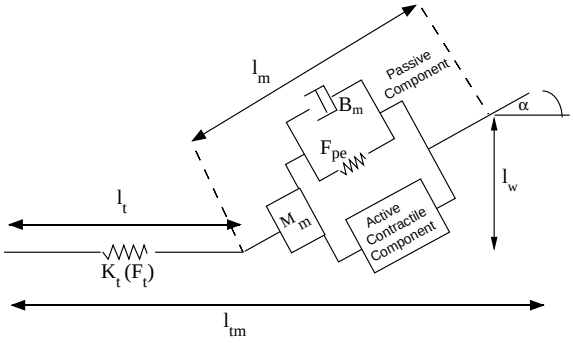

Figure 1. Hill Type Model of the musculotendon complex.

The muscle of length l_m is in series and off-axis by a pennation angle α with the tendon of length l_t. The total pathlength of the musculotendon complex is denoted by l_{tm}. The muscle is assumed to consist of two components: an active force generator and a parallel passive component. The passive component includes a parallel elastic element (F_{pe}) that describes

the passive muscle elasticity and a damping component which corresponds to the passive muscle viscosity (B_m). The model for the active contractile component is based on the generally accepted notion that the active muscle force is the product of three factors: (1) a length-tension relation $f_l(l_m)$, (2) a velocity-tension relation $f_v(\dot{l}_m)$, and (3) the activation level $a(t)$. In this paper, the curves utilized in the modeling of these relations are developed by two methods. In the case that sufficient data is available, a natural cubic spline will be fit to the data. As an alternative approach, analytical expressions that capture the qualitative properties of the curves will be used. The parameters that appear in these expressions will be determined by imposing smoothness conditions in combination with a fit of experimental data.

For multiple muscle systems, such as that used in the simulation of human gait, it is advantageous to develop curves describing the attributes of a generic muscle. This curve can then be scaled with appropriate parameters to reflect the dynamics of a particular muscle. We will see that the scale parameters needed for each musculotendon group include: (1) maximal isometric active muscle force F_o, (2) optimal muscle length, l_o, (3) pennation angle α_o when $l_m = l_o$, and (4) tendon slack length l_{ts}. In developing nondimensional representations for these curves the approach of [31] is implemented and all forces and lengths are scaled as $\tilde{F} = F/F_o$ and $\tilde{l}_m = l_m/l_o$. Another quantity used to specify a muscle specific force-velocity relation is the maximum speed of shortening defined as $v_o \equiv l_o/\tau_c$. This quantity scales time and varies for fast and slow muscles. In the case of the lower extremities a standard value of $\tau_c = .1s$ is used for all muscles types.

Muscle force is easily measured at various lengths under isometric conditions to produce force-length relationships. The curve produced when muscle is not stimulated is the passive force-length curve, $F_{pe}(l_m)$. When muscle is activated the curve that results represents both passive and active contributions. The difference in these two curves is the active force-length relation, $f_l(l_m)$. The length at which the maximum active muscle force, F_o, is developed is called the optimal muscle length, l_o. Figure 2 displays the qualitative nature of these curves.

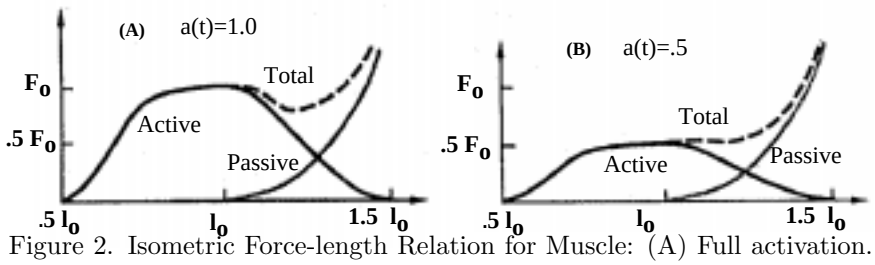

Figure 2. Isometric Force-length Relation for Muscle: (A) Full activation. (B) Active force scales with activation but passive is force is unaffected (adapted from [31]).

A theoretical explanation for the active f_l relation is based on the microscopic nature of muscle and is explained by the Sliding Filament Theory [23]. This theory offers an explanation for the generally accepted notion that when a muscle is completely tetanized, the active force displays a parabolic dependence on length in a nominal region, $.5 \leq \tilde{l}_m \leq 1.5$ with a maximum value of F_o when $l_m = l_o$. At less than full activation, the force-length dependence is obtained by scaling the fully activated f_l curve [31]. In this paper, the active force length relation for muscles of the lower extremities are constructed as a natural cubic spline that fits data reported by [10]. This curve is then scaled to provide a description for specific muscle. For the ocular system, an analytical model of the force length effect is utilized. Several approaches have been suggested, for example [14], but a simple normalized form that is utilized here is

$$f_l(\bar{l_m}) = F_o\left(1 - ((\bar{l_m} - 1)/0.5)^2\right).$$

The nonlinear passive dependence of muscle force on length is described by the function $F_{pe}(l_m)$. Just as in the case of the active force length, the passive force length curves are constructed as cubic splines or modeled by analytical expressions. A commonly used form for F_{pe} and that which is employed here is given in [15] and is expressed as

$$F_{pe}(l_m) = \begin{cases} \left(\frac{k_{ml}}{k_{me}}\right)\left[\exp(k_{me}(l_m - l_{ms})) - 1\right] & l_{ms} \leq l_m < l_{mc} \\ k_{pm}(l_m - l_{mc}) + F_{mc} & l_m > l_{mc} \\ 0 & \text{otherwise.} \end{cases} \tag{2.1.1}$$

The passive muscle slack length is l_{ms} and corresponds to a length at which no force is generated. The transition length from the linear to nonlinear regime is l_{mc} corresponding to a force of F_{mc}. The specific methods by which these parameters as well as the stiffness and shape parameters k_{me}, k_{pm}, k_{ml} are determined from data relevant to a specific application.

Active muscle force is also dependent on muscle velocity. When a muscle actively shortens, it produces less force than it would under isometric conditions. A.V. Hill [17] was the first to quantify this result with an empirical hyperbolic relationship when a muscle is shortening as

$$f_v(v_m) = F_o\frac{v_o - v_m}{v_o + cv_m}$$

where $v_m = \dot{l_m}$ and shortening corresponds to $v_m > 0$. In contrast to a concentric contraction, when a muscle is actively lengthening it is able to produce forces above the maximal isometric force. Experimental data reveals that this relationship is not an extension of Hill's equation and exhibits a threshold which limits the amount of tension muscle can withstand,

approximately $1.8F_o$. The f_v curve is also thought to scale with activation and is displayed in Figure 3. For the muscles involved in the gait model the force velocity curve is constructed as a natural cubic spline fit to data collected while the muscle lengthened and shortened [10]. For the ocular system, an analytical model of f_v is utilized. Due to the way the curve is utilized in the formulation of the dynamics, it is convenient to express this relation in terms of the inverse $f_v^{-1}(F)$. The output of the inverse is normalized with respect to v_o, the maximum speed of shortening. In particular if $\tilde{F}$ denotes a normalized active muscle force,

$$\tilde{v}^m = v^m/v^o = f_v^{-1}(\tilde{F}).$$

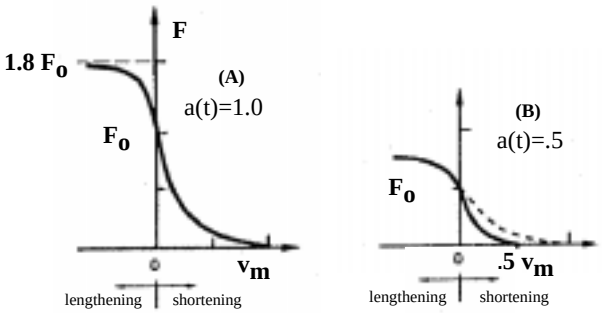

Figure 3. Force-velocity relation for muscles: (A) Full activation when $l_m = l_{mo}$. (B) The force-velocity scales with activation.

There is evidence to suggest that total active force generation is best described by a force-length-velocity relationship which is usually quantified as the product of the force-length and force-velocity curves [31] where the resulting surface is scaled by muscle activation. Consequently, it is convenient to visualize force generation as a collections of surfaces described in terms of nondimensionalzed force velocity and force length curve,

$$F_{act} = a(t)F_0 f_l(\tilde{l_m}) f_v(\tilde{v_m}).$$

Muscle activation, $a(t)$, is related to the neural neural input, $n(t)$, by a process known as contraction dynamics. Both quantities, $n(t)$ and $a(t)$, can be related to experimental data. In particular $n(t)$ is related to rectified EMG while $a(t)$ is related to filtered, rectified EMG [31]. The process through which neural input is transformed into activation is known to be mediated through a calcium diffusion process and is represented by the first order differential equation

$$\frac{da(t)}{dt} + \left[\frac{1}{\tau_{act}}\ (\beta + (1-\beta)u(t))\right]\ a(t) = \frac{1}{\tau_{act}}\ u(t)$$

where $0 < \beta < 1$ and τ_{act} is an activation time constant that varies with fast and slow muscle.

The series elastic element in Figure 1 corresponds to the muscle tendon. More precisely, the tendon is assumed to behave non-linearly under minimal extension and then to become linear with stiffness constant k_s beyond a given length l_{tc} associated with a particular level of resisting force, F_{tc}. A common approach to tendon dynamics (see, for example [15]) is to assume a model of the form

$$\dot{F}_t = K_t(F_t)\dot{l}_t \tag{2.1.2}$$

where

$$K_t(F_t) = \begin{cases} k_{te}F_t + k_{tl} & 0 \leq F_t < F_{tc} \\ k_s & F_t \geq F_{tc} \end{cases}.$$

By integrating the above equation the tendon force can be alternatively expressed as a function of tendon length l_t as

$$F_t(l_t) = \begin{cases} \left(\frac{k_{tl}}{k_{te}}\right)\left[\exp\left(k_{te}(l_t - l_{ts})\right) - 1\right] & l_{ts} \leq l_t < l_{tc} \\ k_s(l_t - l_{tc}) + F_{tc} & l_t > l_{tc} \\ 0 & \text{otherwise} \end{cases} \tag{2.1.3}$$

where l_{ts} denotes tendon slack length. By imposing smoothness conditions on this curve and some notion of fit to experimental data, the shape and stiffness parameters can be specified. However, for the gait model it is convenient to use a generic force-length relationship for tendon derived by a method discussed in [31]. In particular, define tendon strain by $\varepsilon^t = (l_t - l_{ts})/l_{ts}$ and normalized tendon force as $\tilde{F}_t = F_t/F_o$. We assume a generic force-strain curve ($\tilde{F}_t$ vs ε^t) based on the assumptions that a nominal stress-strain curve can be formulated that represents all tendon and that the strain in a tendon when force in the tendon equals the maximal isometric muscle force is independent of the musculotendon unit. By scaling the generic force-strain relationship by F_o and l_{ts}, a force-length function is found for a specific tendon. If we adopt the notion that the tendon behaves as an exponential spring and fit an analytical model as in equation (2.1.3) to data reported by [10], a generic force-strain relationship may be obtained in the form

$$F_t(\varepsilon^t) = \begin{cases} .10377\left(e^{91\varepsilon^t} - 1\right) & 0 \leq \varepsilon^t < .01516 \\ 37.526\varepsilon^t - .26029 & .01516 \leq \varepsilon^t < .1 \end{cases}. \tag{2.1.4}$$

If the strain in tendon reach values beyond .1, the tendon is known to rupture [31]. Since such an extreme value of strain should not occur during

normal locomotion, this part of the curve need not be included in our analysis. From (2.1.4) it follows that tendon stiffness defined by $K_t(F_t) = dF_t/dl_t$ is given by

$$\begin{aligned} K_t(F_t) &= \frac{dF_t}{d\tilde{F}_t} \cdot \frac{d\tilde{F}_t}{d\varepsilon^t} \cdot \frac{d\varepsilon^t}{dl_t} \\ &= \frac{F_o}{l_{ts}} \cdot \frac{d\tilde{F}_t}{d\varepsilon^t} \\ &= \begin{cases} \left(\frac{F_o}{l_{ts}}\right) 91(\tilde{F}_t + .10377) & 0 \le \tilde{F}_t \le .3086 \\ \left(\frac{F_o}{l_{ts}}\right) 37.526 & \tilde{F}_t \ge .3086 \end{cases} \\ &= \left(\frac{F_o}{l_{ts}}\right) K_t(\tilde{F}_t). \end{aligned} \tag{2.1.5}$$

2.2 Contraction Dynamics

From Figure 1 it readily follows that the total force of a muscle is the sum of the passive and the active forces, $F_m = F_{pe} + F_{act} + B_m\dot{l}_m$. Muscle is known to maintain a constant volume and so l_w is constant. With this observation and since

$$l_{mt} = l_t + l_m \cos\alpha,$$

it follows

$$\dot{\alpha} = -\frac{\dot{l}_m}{l_m} \tan\alpha.$$

and

$$\dot{l}_t = \dot{l}_{mt} - \frac{\dot{l}_m}{\cos\alpha}.$$

The tendon dynamics may now be expressed as

$$\dot{F}_t = K_t(F_t)(\dot{l}_{tm} - \dot{l}_m/\cos\alpha). \tag{2.2.6}$$

The equation of motion for the muscle mass is

$$M_m \frac{d^2(l_m \cos\alpha)}{dt^2} = F_t - [F_{act} + F_{pe} + B_m\dot{l}_m]\cos\alpha$$

and with some simple manipulations, the muscle dynamics take the form

$$M_m\ddot{l}_m = F_t\cos\alpha - \cos^2\alpha[F_{act} + F_{pe} + B_m\dot{l}_m] + \frac{M_m\dot{l}_m^2 \tan^2\alpha}{l_m}. \tag{2.2.7}$$

Two state variables are required to describe the contraction dynamics of the musculotendon actuator as given by (2.2.6) and (2.2.7). For multiple muscle systems such as that needed to describe gait, it is desirable to reduce

the system dimension. This can be achieved by eliminating the muscle mass. In this case, (2.2.7) becomes a statement of force balance

$$F_t = F^m \cos\alpha = \left(F_o a(t) f_l(\tilde{l}_m) f_v(\tilde{v}^m) + F_{pe}(\tilde{l}_m) + B_m \dot{l}_m\right) \cos\alpha.$$

If it is assumed that the passive muscle viscosity effect is small, then $\dot{l_m}$ can be computed from

$$\dot{l}_m = v^m = v_o f_v^{-1} \left(\frac{(F_t/\cos\alpha) - F_{pe}(\tilde{l}_m)}{F_0 a(t) f_l(\tilde{l}_m)} \right).$$

It now follows from (2.2.6) and that the differential equation describing the contraction dynamics of the musculotendon is

$$\frac{dF_t}{dt} = \frac{F_0}{l_{ts}} K^t(\tilde{F}_t) \left[\dot{l}_{mt} - \frac{v_o}{\cos\alpha} f_v^{-1} \left(\frac{(F_t/\cos\alpha) - F_0 f_p(\tilde{l}_m)}{F_0 a(t) f_l(\tilde{l}_m)} \right) \right] \qquad (2.2.8)$$

where

$$\begin{aligned}
&v_o = (1/\tau_c) l_0 \\
&\tilde{l}_m = l_m / l_0 = \sqrt{(l_{mt} - l_t)^2 + (l_w)^2}/l_0, \\
&l_t = \begin{cases} l_{ts}\left(1 + \ln\left(\tilde{F}_t/.10377 + 1\right)/91\right) & 0 \le \tilde{F}_t \le .3086 \\ l_{ts}\left(1 + (\tilde{F}_t + .26029)/37.526\right) & .3086 \le \tilde{F}_t \end{cases}, \\
&\cos\alpha = (l_{mt} - l_t)/l_m, \\
&\tilde{F}_t = F_t/F_0.
\end{aligned}$$

3 Ocular Dynamics

In human binocular vision the movement of each eye is controlled by a set of six muscles. When the eyes are fixed on an object two things occur. First, the eye rotates so that the image of the object formed by the eyes' lens system is projected onto the fovea of the retina. This is the area of the retina of greatest ocular acuity. Secondly, the eye lenses adjust to bring the object into focus. This section is concerned with the first part of this process: how the rotation develops and how it is controlled. The brain and central nervous system process information obtained by the retina, and then transmit signals to the extraocular muscles. These muscles work in three agonist-antagonist pairs to exert forces on the eye causing it to rotate.

The three muscle pairs consist of the medial and lateral recti, the superior and inferior recti, and the superior and inferior obliques. The lateral

and medial recti produce primarily horizontal rotation. The superior and inferior recti work mainly to control vertical rotation. The superior oblique controls the intorsional rotation (toward the nose) of the eye while the inferior oblique controls mainly extorsional rotation (toward the temple). The eye has three degrees of freedom but experimental evidence shows that for any horizontal rotation (θ) and vertical rotation (ϕ), the amount of torsional rotation (ψ) is determined by a phenomena known as Listing's Law,

$$\psi = \arccos\left(\frac{\sin\theta\sin\phi}{1+\cos\theta\cos\phi}\right).$$

The motion of the eye is a result of moments produced by the six extraocular muscles and a passive moment due to the orbit which restrains the rotation of the globe. If $\omega_x,\ \omega_y,\ \omega_z$ denote the components of angular velocity with respect to a fixed inertial reference frame with coordinates x, y, z, then the equation of motion for the globe is of the form

$$\begin{pmatrix} \dot{\omega_x} \\ \dot{\omega_y} \\ \dot{\omega_z} \end{pmatrix} = \frac{1}{J_G}\Big[(\vec{r_{lr}}\times\vec{F_{lr}}) + (\vec{r_{mr}}\times\vec{F_{mr}}) + (\vec{r_{sr}}\times\vec{F_{sr}}) \qquad (3.0.1)$$
$$+ (\vec{r_{ir}}\times\vec{F_{ir}}) + (\vec{r_{so}}\times\vec{F_{so}}) + (\vec{r_{io}}\times\vec{F_{io}}) + (\vec{rp}\times\vec{F_p})\Big].$$

Here $\vec{r_{lr}}$ and$\vec{F_{lr}}$ denote the moment arm and force associated with the lateral rectus, with the obvious interpretation of the other terms. Three dimensional simulations carried out in [22] support the claim that horizontal eye movement may be accurately modeled by including only the medial and lateral rectus muscles. We will assume that the points of attachment are such that the moment these muscles generate is in the direction of the z axis (see Figure 4).

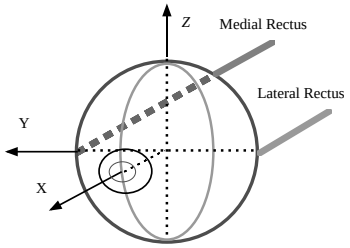

Figure 4. Left globe with medial and lateral rectus muscles.

More specifically, the model presented here will be restricted to horizontal saccadic eye movements. The purpose of saccadic eye movement is to position the high-resolution fovea, the central part of the retina, on the important features of a scene. This is achieved by altering the direction and

magnitude of the saccade so as to correct for position error. Because saccades are among the fastest muscle movements that are performed, vision is suppressed during this motion and it is generally accepted that the the oculomotor system operates in an open-loop mode when performing a saccadic movement. The model proposed herein builds upon earlier models of the oculomotor system [2, 6]. However, the model presented here incorporates more general formulations of the musculotendon dynamics as presented in the previous section and allows for the inclusion of muscle mass. There are several reasons that a meaningful model of the horizontal saccadic movement system can be developed. Experimental data has been gathered that provides values for many of the parameters that arise in the description of the model. Most importantly in this regard is information regarding the time course of innervation that is specific to saccadic movement. Experimental data provides fairly conclusive information regarding the nature of the inputs, or controls, that are appropriate to saccades. More specifically, the input into the oculomotor plant is derived from experimental records of raw EMG corresponding to the firing rate of motor units. It is accepted as 'sufficiently realistic as to be useful' [25] that the rate of discharge corresponding to a saccadic movement can be described by filtered EMG that corresponds to a rectangular pulse followed by a step.

Figure 5 provides a mechanical representation of the eye plant model in which the elements of the plant are displayed as if the muscles and the globe are undergoing linear motion. One must distinguish between the lateral rectus, (the agonist) and the medial rectus (the antagonist). All model components that pertain to the agonist will be denoted as $F_{t1}, l_{tm1}, B_{m1}, M_{m1}$, etc, while the corresponding quantities for the agonist are indicated by $F_{t2}, l_{tm2}, B_{m2}, M_{m2}$, etc.

Figure 5. The model of the eye plant.

Because of conventions adopted in the ocular literature, it is convenient to report rotations of the eye in degrees (°) and to write the equation of motion for the globe and the musculotendon dynamics in terms of pure tendon force in units of grams tension. To this end let J_G, B_G, and K_G denote the parameters for globe inertia, globe viscosity, and globe elasticity, respectively, in terms of cgs units and radians. Let r denote the radius of the globe and define

$$J_g = \frac{J_G}{980r(180/\pi)}, \quad \text{in gt} \cdot \text{s}^2/^\circ$$

and similarly for B_g, K_g. If F_{t1} and F_{t2} are reported in gt, then equation (3.0.1), when expressed in degrees and units of gt, becomes

$$J_g\ddot{\Theta} + B_g\dot{\Theta} + K_g\Theta = F_{t1} - F_{t2}.$$

If pennation effects are ignored, the equation of motion for the muscle mass of the agonist and antagonist, previously expressed in (2.2.70, now takes the form for $i = 1, 2$

$$\frac{M}{980}\ddot{l}_{mi} + B_{pm}\left(\frac{180}{\pi r}\right)\dot{l}_{m1} = F_{ti} - F_{acti} - F_{pe1}(l_{mi}).$$

In a similar fashion, the tendon dynamics and the description of the passive muscle elasticity must be amended to account for the change in units. In particular, the modified forms of (2.1.1),(2.1.2) are

$$F_{pe}(l_m) = \begin{cases} \left(\frac{k_{m1}}{k_{me}}\right)\left[\exp(k_{me}\left(\frac{180}{\pi r}\right)(l_m - l_{ms})) - 1\right] & l_{ms} \le l_m < l_{mc} \\ k_{pm}\left(\frac{180}{\pi r}\right)(l_m - l_{mc}) + F_{mc} & l_m > l_{mc} \\ 0 & \text{otherwise} \end{cases}$$

and

$$\dot{F}_t = K_t(F_t)\left(\frac{180}{\pi r}\right)\dot{l}_t$$

with the obvious change in (2.1.3). For the agonist, the tendon dynamics become,

$$\dot{F_{t1}} = K_t(F_{t1})\left[-\dot{\Theta} - \left(\frac{180}{\pi r}\right)\dot{l}_{m1}\right]$$

while for the agonist,

$$\dot{F_{t2}} = K_t(F_{t2})\left[\ \dot{\Theta} - \left(\frac{180}{\pi r}\right)\dot{l}_{m2}\right].$$

If a state vector is selected as

$$\mathbf{x}^T(t) = \left[\ \Theta \quad \dot{\Theta} \quad l_{m1} \quad \dot{l}_{m1} \quad l_{m2} \quad \dot{l}_{m2} \quad F_{t1} \quad F_{t2} \quad a_1 \quad a_2\ \right],$$

the state equations for the system are given by

$$\dot{\mathbf{x}}(t) = \begin{bmatrix} x_2 \\ \frac{1}{J_g}(x_7 - x_8 - B_g x_2 - K_g x_1) \\ x_4 \\ \frac{980}{M}(x_7 - F_{act}(x_3, x_4, x_9) - F_{pe}(x_3) - B_{pm}(\frac{180}{\pi r})x_4) \\ x_6 \\ \frac{980}{M}(x_8 - F_{act}(x_5, x_6, x_{10}) - F_{pe}(x_5) - B_{pm}(\frac{180}{\pi r})x_6) \\ K_t(x_7)\left[-x_2 - \left(\frac{180}{\pi r}\right)x_4\right] \\ K_t(x_8)\left[\ x_2 - \left(\frac{180}{\pi r}\right)x_6\right] \\ \frac{1}{\tau_1(t)}[\,n_1(t) - x_9] \\ \frac{1}{\tau_2(t)}[n_2(t) - x_{10}] \end{bmatrix}$$

The simulations illustrated in Figure 6 originate from the primary position and the initial conditions for muscle length, tendon force, and activation are taken from [25]. The vector of initial data is then $\mathbf{x}^{\mathsf{T}}(0) = [0\ 0\ 4\ 0\ 4\ 0\ 20\ 20\ .17\ .17]$.

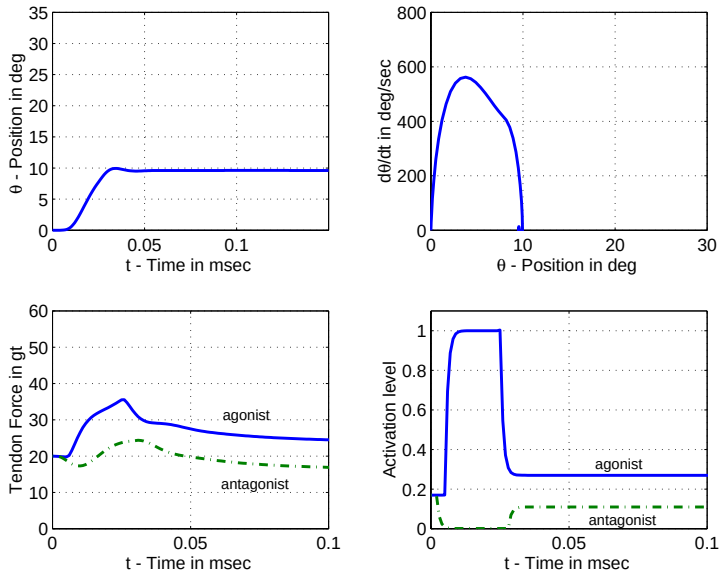

Figure 6. Model simulation of 10 degree saccade.

The simulated trajectory, velocity, and tendon force are in close agreement with the empiric data of [7, 25]. The results of Figure 7 illustrate the effects of pulse-width and pulse-height mismatch in glissadic overshoot and undershoot. The results show that the pulse-height errors are associated with unusually large peak velocities. In contrast, pulse width mismatches produce saccades with reasonable predictions of velocities. These results are in qualitative agreement with experimental results of [3] which suggest that when glissadic overshoot is associated with low peak velocities, the error is caused by the erroneous neural input in computing the pulse width, not the height.

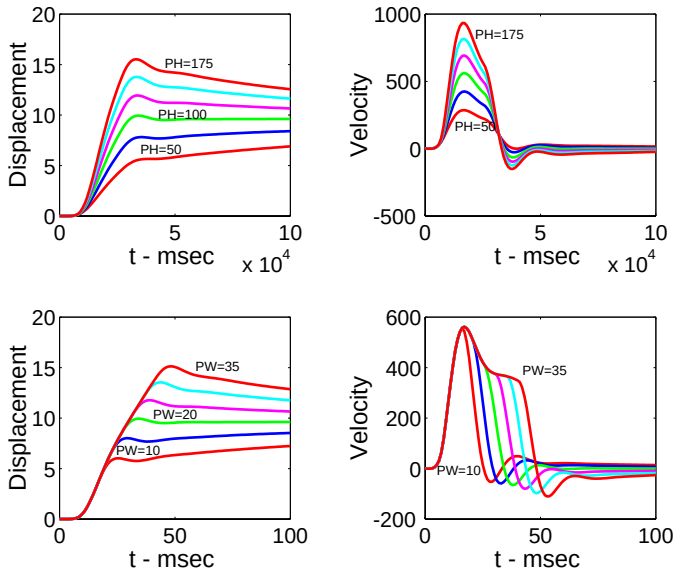

Figure 7. Glissadic overshoot due to pulse width and height errors.

4 A Forward Dynamic Model of Gait

In order to generate the loading conditions during gait, it is necessary to develop a model driven by musculotendon actuators that simulates normal gait. Although many gait models have been built, few include the complexity which is needed for realistic dynamic simulations. The approach that is adopted here builds on a model developed by [30]. The model constrains seven rigid-body segments which represent the feet, shanks, thighs and trunk to 8 degrees of freedom. All joints are assumed to be revolute

having one degree of freedom with the exception of the stance hip which has two degrees of freedom. This allows the hip to ab/adduct, a condition which reduces the degree of coupling between the trunk and the swing leg. Figure 8 shows the generalized coordinates used to describe the configuration of the body. Joint angles q_1, q_2, and q_3 are measured with respect to the horizontal or transverse plane and the rotation of these joints occur about an axes parallel to $\vec{n}_2$. Movement of the stance leg is confined to the sagittal plane, but due to the extra degree of freedom granted to the stance hip, the swing leg and trunk can also move in the frontal or coronal plane through pelvic list. Joint angle q_4 tilts the trunk as well as the swing leg about an axis parallel to $\vec{n}_1 = \vec{d}_1$. Joint angles q_5 through q_8 are measured in the tilted plane and these rotations occur about an axis parallel to $\vec{d}_2$.

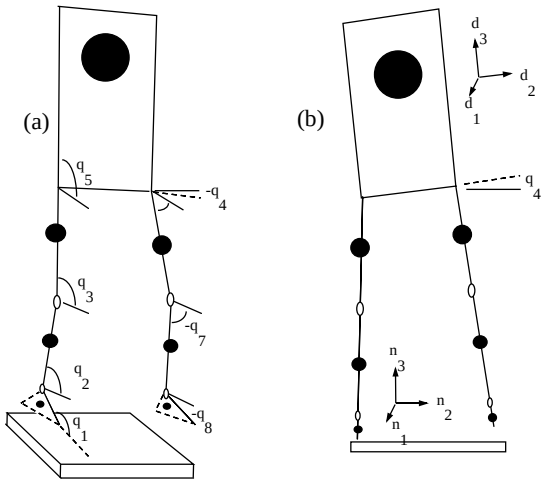

Figure 8. 3-D, 8 DOF Model Showing Segment Angle Definitions: (a) The stance hip has two DOF, while all other joints are revolute. (b) Front view showing pelvis list. Stance angles are specified with respect to the inertial frame, $\vec{n}$, while the swing angles are respect to the titled trunk reference frame, $\vec{d}$ (Adapted from [30]).

This musculoskeletal model represents a normal male with mass totaling 76 kilograms. Segmental dimensions and inertial parameters used in the model are presented in [11]. A key element of the model is that only one-half (14%, approximately left-toe-off, to 62%, approximately left-foot-flat) of the gait cycle is simulated in this analysis. The complete gait cycle can be reconstructed under the assumption of bilateral symmetry. This assumption simplifies the modeling in that the stance leg is always the

stance leg and the swing leg is always the swing leg. As a result, muscles in the swing and stance leg can vary according to the function of that leg in the simulation. With this assumption, it is also valid to have the stance toe constrained to the ground which eliminates one more degree of freedom. This simplification requires fewer muscles to be modeled and reduces the system dimension.

The range of each joint angle is limited to normal ranges through the use of ligamentous constraints. If the joint angle stays within a nominal range, then the effects of the passive structure are minimal, but when the nominal range is exceeded, the passive torques grow exponentially. The general form of the passive moments is given by

$$M_{pass} = k_1\, e^{-k_2(\theta-\theta_2)} - k_3\, e^{-k_4(\theta_1-\theta)} - c\,\dot{\theta}.$$

Here θ is the joint angle measured in radians, $\dot{\theta}$ is the joint velocity measured in radian per second and M_{pass} is measured in Newton-meters. Note that $\theta_2 < \theta < \theta_1$ represents a nominal range for that joint. Initial estimates of the parameters k_j, θ_j, and c were taken from [9] and then modified in the course of validating the model. The inclusion of the passive term $(-c\,\dot{\theta})$ is vital since the passive viscosity was excluded from the the musculotendon model when mass was eliminated. A list of the passive parameters and definitions of the joint angles in terms of the generalized coordinates is given in [11].

Although the stance toe is constrained throughout the simulation, it is necessary to incorporate additional constraints in order to prevent the stance heel and swing foot from penetrating the "ground" and to eliminate excess sliding of the swing foot during double support. These additional constraints are considered to be soft [16]. The vertical ground reaction forces which act on the heels of both the stance and swing leg are modeled as highly-damped, stiff linear springs

$$F_{normal} = \begin{cases} 0 & zheel \geq 0 \\ -(1.5\times 10^5)zheel - (1\times 10^3)\dot{zheel} & zheel < 0 \end{cases}$$

where $zheel$ is the height of the heel above the ground. On the swing heel an additional frictional force applied in a direction parallel to the ground in the sagittal plane is used to prevent excess sliding. This force is proportional to the normal force applied to the swing heel,

$$F_{friction} = \begin{cases} 0 & zheel_{swing} \geq 0 \\ -.5|F_{normal}(zheel_{swing})| & zheel_{swing} < 0 \end{cases}.$$

Once flat-foot is achieved by the swing leg, a counterclockwise torque is applied to prevent the foot from penetrating the ground. The torque is model as a damped, torsional spring which resists plantarflexion of the

foot. This torque is given by

$$T = \begin{cases} 0 & zheel_{swing} > 0 \text{ or } \delta \geq 0 \\ -5696\delta - 38.19\dot{\delta} & zheel_{swing} \leq 0 \text{ and } \delta < 0 \end{cases}$$

where δ is the angle the bottom of the foot makes with the ground. These soft constraints allow the same model to be used during the single and double support phases of gait. If the ground had been modeled as a "hard" constraint, then one would lose a degree of freedom on the swing leg when the toe touches the ground. This would mean two models would be needed to simulate this phase of gait and a switch between the two systems would occur at heel strike.

The model that is developed here incorporates the same muscle sets as that utilized in [30]. As a result, ten musculotendon units are incorporated into our model, five on each leg. On the stance leg, the relevant muscle groups are the soleus, gastrocnemius, vasti, gluteus medius and minimus, and the iliopsoas. The swing leg utilizes the dorsiflexors, hamstring, vasti, gluteus medius and minimus and the iliopsoas. Thus seven different musculotendon groups need to be specified in this model. The constituent muscles composing each musculotendon group, and the parameters which are used to distinguish the dynamics of each particular musculotendon unit, that is, tendon slack length, optimal muscle length, maximal isometric force and pinnation angle, are listed in [11].

In order to incorporate the musculotendon actuators into the dynamics, it is necessary to place the muscles geometrically on the body segment so that the length of the musculotendon, l_{mt}, and the velocity of the musculotendon, v_{mt}, can be derived as a functions of the state variables, i.e. the generalized coordinates, q_i. The attachment of the musculotendon to bone is specified by the defining an origin or proximal attachment, and an insertion or distal attachment. Effective origins and effective insertions are specified when the straight path from the actual origin to actual insertion passes through bone or out of anatomical range during certain body configurations. Origins and insertions are specified with respect to coordinate systems which are directed along the bones and are fixed with respect to the foot, shank, thigh and pelvis. The origin and insertion points for the 7 muscle groups used in this analysis were based on from [5, 18] and are summarized in [11]

The total length and velocity of the musculotendon complex, which is needed as input into the musculotendon dynamics, can be derived for most muscles through vector addition. In this case, the length of the musculotendon is given by

$$l_{mt} = |\overrightarrow{O_a O_e}| + |\overrightarrow{O_e I_e}| + |\overrightarrow{I_e I_a}|$$

where O and I refer to origin and insertion, and the subscripts e and a refer to actual and effective coordinates (Figure 9). The velocity of the musculotendon is then just the time derivative of the length. Musculotendon forces

were incorporated into the body dynamics as joints torques. When a musculotendon spans a joint a torque is realized across that joint. The joint torque due to musculotendons which do not span the knee are computed using standard vector cross product methods. In this case, the moment $\overrightarrow{M}$ acting on the proximal segment is defined as

$$\overrightarrow{M} = \pm F^t \left(\vec{p} \times \frac{\overrightarrow{O_e I_e}}{|\overrightarrow{O_e I_e}|} \right). \tag{4.0.1}$$

Here $\vec{p}$ is a vector from the joint to a point on the line of action of the musculotendon. The line of action is defined by the unit vector $\overrightarrow{O_e I_e}/|\overrightarrow{O_e I_e}|$, and the tension in the musculotendon complex, F^t, is produced according to the muscle dynamics (2.2.8). The sign in equation (4.0.1) depends on whether the musculotendon acts to extend or flex the joint it spans. The cross product,

$$\overrightarrow{m_e} = \vec{p} \times \frac{\overrightarrow{O_e I_e}}{|\overrightarrow{O_e I_e}|},$$

represents the effective moment arm associated with the musculotendon at a certain body configuration.

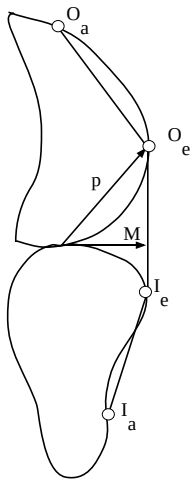

Figure 9. Muscle pathway and effective moment arm.

Vector addition works well for all muscles which do not span the knee. The complication which arises for those musculotendons which do span the knee (vasti, hamstring, and gastrocnemius) occurs because of the complexity of the knee joint. In short, as the knee flexion angle varies, this produces both a change in the location of the knee joint center and in the location of the patella. Since this complexity is not accounted for in the simple

segmental model formulated here, an alternative to the vector method is implemented for the knee. We define the effective moment arms of the vasti, hamstring and gastrocnemius according to curves formulated in [29]. The joint moments produced by these musculotendons which span the knee are given by

$$\vec{M} = \pm F^t \cdot m_e(\theta_f)$$

where F^t is calculated from (2.2.8) and m_e is the effective moment arm as a function of the knee flexion angle, θ_f. The length of these musculotendons is calculated by integration of the moment arm as in [18]. In this method the relationship between the length of the musculotendon, the effective moment arm, and the joint angle is given by

$$v^{mt} = \frac{d\,L^{mt}}{dt} = m_e(\theta_f)\frac{d\,\theta_f}{dt}.$$

Consequently, three more differential equations are added to the system.

When a direct-dynamic analysis of gait is to be simulated, controls for the musculotendon actuators must be derived. Developing these controls constitutes one of the more difficult aspects of a forward analysis. Some form of dynamic optimization is usually utilized in developing the controls. The controls used in the gait simulations of this paper are derived through a two-phase process: (1) a coarse formulation based on a dynamic optimization scheme, and, (2) a fine-tuning via trial-and error. The coarse controls are derived as in [30] by employing a cost function that consists of a error tracking term which penalizes deviations from a desired trajectory and a term related to muscle fatigue [8],

$$J_i(k) = \sum_{l=1}^{16} w_{x,l}(x_l - x_{l,des})^2 + \sum_{l=1}^{m} w_{u,l}\left(\frac{F_{tl}}{A_l}\right)^3. \qquad (4.0.2)$$

In equation (4.0.2), x_l is one of the elements of the state variable, $\vec{X} = (q_1, q_2, \ldots, \dot{q_1}, \dot{q_2}, \dot{q_3}, \ldots)$ (refer to Figure 8), and F_{tl} and A_l are the force and physiological cross-sectional area of muscle l. The nominal gait trajectory is described by $x_{l,des}$ and is specified according to data recorded in [28]. Once crude activation controls are formulated, simulations were run and these controls were fine-tuned by ad-hoc methods to meet the specific needs of our model. The final formulation of the control laws derived for the model varied slightly from those of [30]. The resulting muscle activation is illustrated in Figure 10.

For this study, the algebraic manipulation program AUTOLEV [19] was utilized to derive the equations of motion for the gait simulation. This program implements Kane's method as a means of deriving Euler's equations of motion. A detailed discussion of the procedure by which the equations are derived is given in [11]. It suffices here to point out that AUTOLEV

generates the equations of motion as well as FORTRAN or C code for integrating these equation forward in time using a fourth-order Runge Kutta scheme.

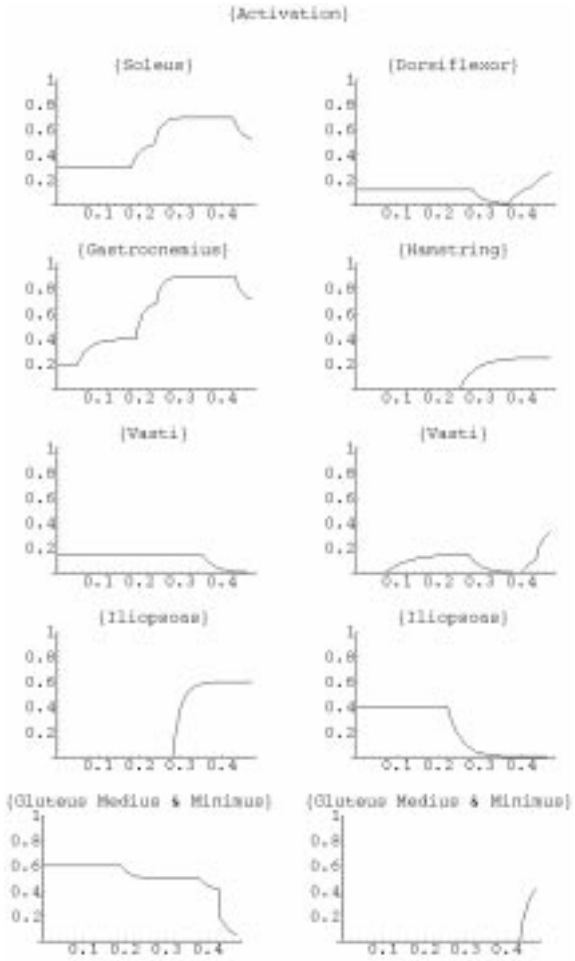

Figure 10. Controls utilized in the gait simulation.

Necessary initial data to run a simulations included the initial segmental orientations $(q_1, ..., q_8)$, the initial angular speeds $(\dot{q}_1, ..., \dot{q}_8)$, the initial force in each musculotendon, and the initial lengths of the musculotendons. Precise values of this data is not readily available and was approximated by several methods. For instance, the initial force in each musculotendon unit was found by running simulations to find the steady state muscle force achieved by the initial control when the motion of the model was constrained. Initial lengths of the musculotendon were estimated so that

the muscle maintained an appropriate length throughout the gait cycle. A summary of initial conditions that were utilized in running gait simulations can be found in [11].

A standard means of comparing and validating gait simulations is achieved by displaying the joint torques which drive the system and the resulting joint trajectories. Figure 11 depicts the standard definitions of the joint angles. Notice that these joint angles are distinct from the generalized coordinates used in the analysis. Figure 12 displays the resulting joint trajectories in the simulation. These trajectories provide good qualitative agreement with the trajectories reported by other researchers (see for example [28]). Joint torques and power trajectories, which reflect the rate at which the muscles and tendons are expending and absorbing energy, were in general accordance with the data reported by other researchers [13, 9].

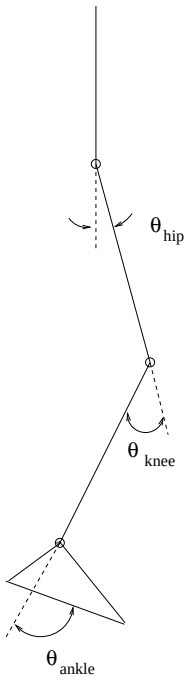

Figure 11. Joint angle definitions.

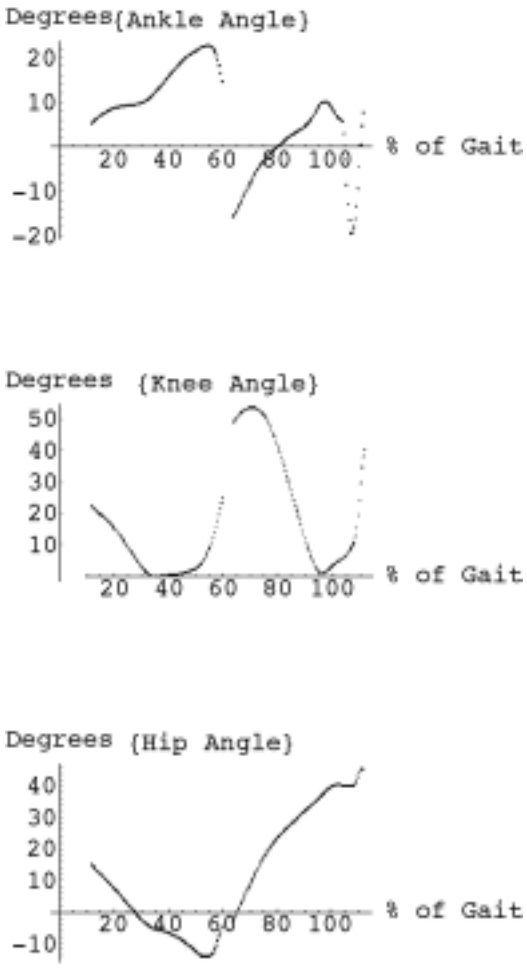

Figure 12. Joint Trajectories.

Figure 13 reports the normalized force realized in the tendons of all ten musculotendon actuators. These normalized forces, F_t/F_0, were obtained through the dynamics in 2.2.8 and are utilized in specifying the loading conditions for the stress analysis. Additional boundary conditions needed for the stress analysis were obtained by appropriately constraining generalize coordinates so that joint reaction forces could be determined.

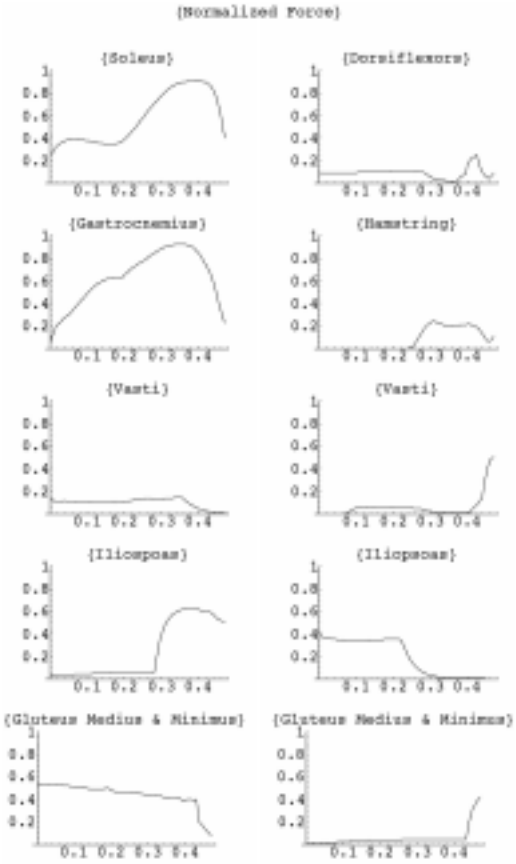

Figure 13. Normalized Force Histories for each musculotendon. Left column refers to stance muscle while the right column refers to the swing side muscles.

4.1 The Stress Analysis

The stress distribution in the long bones of the lower extremities is calculated from equilibrium considerations by 'freezing' the gait model at a fixed instant in time and regarding the segmental elements as linear isotropic elastic bodies. The method that is implemented here follows the approach given in [27]. The applied loads for the stress analysis are the joint reaction forces and the muscle forces as calculated in the gait analysis. The joint reaction forces and joint moments due to musculature effects are resolved into forces and moments at each cross section of the tibia. The components of the stress tensor are calculated in terms of these internal forces and moments.

The relevant geometry is indicated in Figure 14. Assign to the *ith* cross section a local set of orthogonal axes parallel to the unit vectors ζ_i, η_i, ξ_i with the origin at the center of gravity. The following measures of anthropometric data for the each segment for each segmental link must be collected or approximated. Let A_i denote the area of the ith cross section, $(I_\xi)_i$, $(I_\eta)_i$ the statical moments of inertia around the ξ_i and η_i axes, and $(I_{\xi\eta})_i$ the statical product of inertia of the cross sectional area. In the ith section, let w_{ijk} denote the width of the cross section at the point (j,k) parallel to the ξ_i axis, $(W_\xi)_{ijk}$ the moment about the ξ axes of the area bounded by the segment of length w_{ijk} and the perimeter of the cross section, and $(W_\eta)_{ijk}$ the moment about the η axis. (see Figure 14). Similarly, let h_{ijk} denote the height of the cross section at the point (j,k) parallel to the η_i axis and $(H_\xi)_{ijk}$ the moment about the ξ axis of the area bounded by the segment of length h_{ijk} and the perimeter of the cross section with the obvious interpretation of $(H_\eta)_{ijk}$.

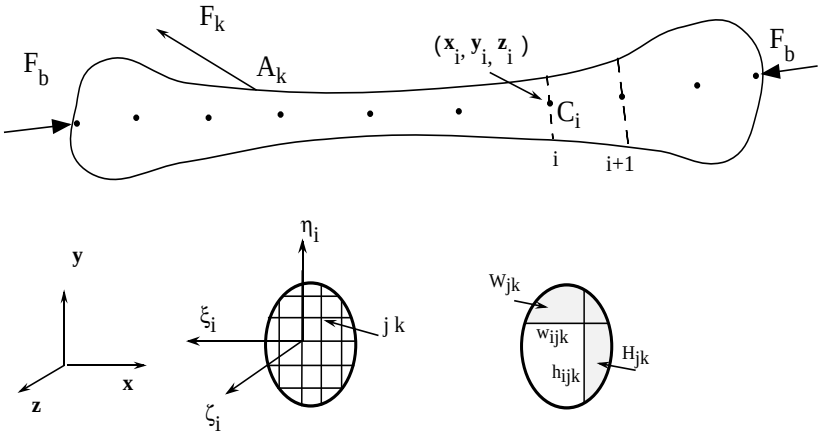

Figure 14. Local coordinates and cross sections of bone.

From equilibrium considerations, the joint reaction forces must be collinear and give rise to an internal force vector on each cross section whose components in terms of the local coordinates are equal and opposite to those of F_b. The component of this internal force acting on the ith cross section is obtained by projection onto the local coordinates. Thus for the ζ direction,

$$(P_\zeta)_i = -F_b \cdot \zeta_i.$$

and similarly for $(P_\eta)_i$ and $(P_\xi)_i$. If $\overrightarrow{C_iC_1}$ denotes the vector from (x_i, y_i, z_i) to (x_1, y_1, z_1), then the component of the reactive moment due to F_b the ζ direction is given by

$$(M_\zeta)_i = -(M)_i \cdot \zeta_i$$

where

$$(M)_i = \overrightarrow{C_i C_1} \times F_b$$

with $(M_\eta)_i$ and $(M_\xi)_i$ defined in a similar way.

If a muscle force acts on the bone, reactive forces and moments at the joints must be introduced to maintain the state of equilibrium. These joint forces and moments will contribute to the internal forces and moments on the cross sections. In particular, suppose a muscle force F_k^m is attached to the bone a point A_k. Introduce joint reaction forces $R_{k1} = (-1/2)F_k^m$ at the points (x_1, y_1, z_1) and (x_n, y_n, z_n). The moment at (x_n, y_n, z_n) due to R_{k1} is

$$M_{k1} = \overrightarrow{C_n C_1} \times R_{k1}$$

and the moment due to the muscle force is

$$M_{k2} = \overrightarrow{C_n A_k} \times F_k^m.$$

To maintain equilibrium in the segment we introduce a reactive moment given by

$$R_{k2} = -(M_{k1} + M_{k2}).$$

The internal forces on a cross section due to R_{k1} are computed in the same manner as for the joint reaction force by simply replacing F_b with R_{k1}. The corresponding internal moment on a section C_i between C_1 and A_k is

$$(M_k)_i = (\overrightarrow{C_i C_1} \times R_{k1}) - R_{k2}.$$

If the section is between A_k and C_n, replace $\overrightarrow{C_n A_k}$ by $\overrightarrow{C_1 A_k}$. When several muscles act on the segment, the computations are repeated for each muscle and the effect of all muscles is then obtained by summing contributions of each force. The total internal forces due to the combined effect of the joint reaction force and all muscle attachments is

$$(P_\zeta)_i = -F_b \cdot \zeta_i - \sum_k R_{k1} \cdot \zeta_i$$

and similarly for $(P_\eta)_i$ and $(P_\xi)_i$. The total internal moments are

$$(M_\zeta)_i = -M_i \cdot \zeta_i - \sum_k (M_k)_i \cdot \zeta_i$$

with the obvious expressions for $(M_\eta)_i$ and $(M_\xi)_i$.

If the bone is assumed to be in a state of biaxial bending, the stress tensor has the general form

$$S_{ijk} = \begin{bmatrix} (\sigma_\zeta)_{ijk} & (\tau_{\zeta\eta})_{ijk} & (\tau_{\zeta\xi})_{ijk} \\ (\tau_{\zeta\eta})_{ijk} & 0 & 0 \\ (\tau_{\zeta\xi})_{ijk} & 0 & 0 \end{bmatrix}.$$

The normal stresses due to the compressive and bending forces are computed from well-known formulas concerning biaxial bending and are given by

$$(\sigma_\zeta)_{ijk} = (\sigma_c)_{ijk} + (\sigma_b)_{ijk},$$

where

$$(\sigma_c)_{ijk} = \frac{(P_\zeta)_i}{A_i},$$

$$(\sigma_b)_{ijk} = \frac{[(M_\eta)_i(I_\xi)_i + (M_\xi)_i(I_{\eta\xi})_i]\xi_{ijk} - [(M_\eta)_i(I_{\eta\xi})_i + (M_\xi)_i(I_\eta)_i]\eta_{ijk}}{B_i},$$

$$B_i = (I_\eta)_i(I_\xi)_i - (I_{\eta\xi})_i,$$

and ξ_{ijk}, η_{ijk} are the distances from (j,k) to the ξ and η axes respectively. The shearing stresses are given by

$$(\tau_{\zeta\eta})_{ijk} = (\tilde{\tau}_{\zeta\eta})_{ijk} + (\hat{\tau}_{\zeta\eta})_{ijk}, \qquad (\tau_{\zeta\xi})_{ijk} = (\tilde{\tau}_{\zeta\xi})_{ijk} + (\hat{\tau}_{\zeta\xi})_{ijk}$$

where

$$(\hat{\tau}_{\zeta\eta})_{ijk} = \frac{(\tau_\zeta)_{ijk}\xi_{ijk}}{\sqrt{(\eta_{ijk})^2 + (\xi_{ijk})^2}}, \quad (\hat{\tau}_{\zeta\xi})_{ijk} = -\frac{(\tau_\zeta)_{ijk}\eta_{ijk}}{\sqrt{(\eta_{ijk})^2 + (\xi_{ijk})^2}},$$

$$(\tau_\zeta)_{ijk} = \frac{(M_\zeta)_i\sqrt{(\eta_{ijk})^2 + (\xi_{ijk})^2}}{(I_\eta)_i + (I_\xi)_i},$$

$$(\tilde{\tau}_{\zeta\xi})_{ijk} = \frac{[(P_\eta)_i(I_\eta)_i - (P_\xi)_i(I_{\eta\xi})_i](H_\xi)_{ijk} + [(P_\xi)_i(I_\xi)_i - (P_\eta)_i(I_{\eta\xi})_i](H_\eta)_{ijk}}{h_{ijk}B_i},$$

and

$$(\tilde{\tau}_{\zeta\eta})_{ijk} = \frac{[(P_\eta)_i(I_\eta)_i - (P_\xi)_i(I_{\eta\xi})_i](W_\xi)_{ijk} + [(P_\xi)_i(I_\xi)_i - (P_\eta)_i(I_{\eta\xi})_i](W_\eta)_{ijk}}{w_{ijk}B_i}.$$

In Figures 15-16 the normal stress, (σ_ζ), at heel strike and flat foot is computed on the medial, lateral, anterior, and posterior cortex of the tibia, and plotted versus length of the tibia, from the proximal to distal end. The stress in the absence of muscular effects is indicated by (NM). The results show that muscular loads have a dramatic effect on the stress distribution. Computations based on joint reaction forces alone would underestimate stresses by an order of magnitude. With the inclusion of muscular attachment, the predicted stress is in qualitative agreement with the results of [21] in that tensile stresses are generally greater at flat foot as compared to heel strike. The results are not surprising in view of the fact that muscular forces often exceed body weight and thus dominate the loading on bones both at the joints and at the point of muscle attachment.

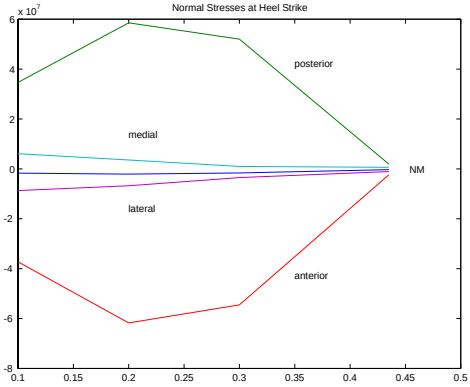

Figure 15. The normal component of stress in the axial direction of the tibia at heel strike.

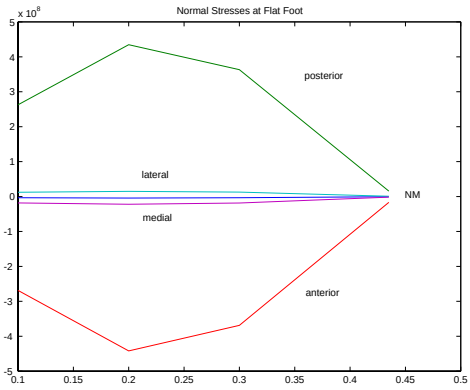

Figure 16. The normal component of stress in the axial direction of the tibia at flat foot.

References

[1] Audu, M.l., and Davy, D.T. The influence of muscles model complexity in musculoskeltal motion modeling. *J. Biomech. Engrg.*, **107**: 147-157 (1985).

[2] Bahill, A., Latimer, J., and Troost, B. Linear homeomorphic model for human movement. *IEEE Trans. Biomed. Eng.*, Vol. BME-27, No. 11, (1980).

[3] Baloh, R. W., etal. Internuclear Opthalmoplegia. *Archives of Neurology*, Vol. 35, pp. 484-493, (1978).

[4] Biewener, A.A. *Biomechanics Structures and Systems: A Practical Approach*, Oxford University Press, New York (1992).

[5] Brand, R.A., Crowninshield, R.D., Wittstock, C.E., Pedersen, D.R., Clark, C.R., and Van Krieken, F.M. A model of lower extremity muscular anatomy.*J. Biomech. Engrg.*, **100**: 88-92 (1982).

[6] Clark, M. R., and Stark, L. Control of human eye movements: I. Modelling of extraocular muscles; II. A model for the extraocular plant mechanism; III. Dynamic characteristics of the eye tracking mechanism. *Mathematical Biosciences*, Vol. 20, pp. 91-265, (1974).

[7] Collins, C. Orbital Mechanics. In P. Bach-y-Rita, C. Collins, Eds., *The Control of Eye Movements*, Academic Press, New York, p. 283 (1973).

[8] Crowninshield, R.D., Brand, R.A. (1981) A physiologically based criterion of muscle force prediction on locC.omotion.*J. Biomechanics.*, **14**: 793-801.

[9] Davy, D.T., and Audu, M.l. A dynamic optimization technique for predicting forces in the swing phase of gait.*J. Biomechanics.*, **20**: 187-202 (1987).

[10] Delp, S.L., Loan, J.P., Hoy, M.G., Zajac, F.E., Topp E.L., Rosen, J.M. An interactive graphics-based model of the lower extremity to study orthopaedic surgical procedures. *IEEE Transactions on Biomedical Engineering.* **37**: 757-767 (1990).

[11] DeWoody, Y., The role of muscular skeletal dynamics and neuromuscular control in stress development in bone. *Ph.D. Dissertation*, Department of Mathematics and Statistics, Texas Tech University (1998).

[12] Gordon, A.M., Huxley, A.F., and Julian, F.J. Tension development in highly stretched vertebrate muscle fibres. *J. Physiol.*, **184**: 143-169 (1966).

[13] Hardt, D.E. Determining muscle forces in the leg during normal human walking – An application and evaluation of optimization methods.*J. Biomech. Engrg.*, **100**: 72-78 (1978).

[14] Hatze, H. The complete optimization of human motion. *Math. Biosci.*, **28**: 99 (1976).

[15] He, J. A feedback control analysis of the neuro-musculo-skeletal control system of a cat hindlimb. *Ph.D. Dissertation*, Department of Electrical Engineering, University of Maryland (1988).

[16] Hemami, H., Jaswa, V.C., and McGhee, R.B. Some alternative formulations of manipulator dynamics for computer simulation studies. *Prc. 13th Allerton Conf. on Circuit Theory,* University of Illinois, (1975).

[17] Hill, A.V. The heat of shortening and dynamic constants of muscle. *Proc. Roy. Soc. B.*, **126**: 136-195 (1938).

[18] Hoy, M.G., Zajac, F.E., and Gordon, M.E. A musculoskeletal model of the human lower extremity: The effects of muscle, tendon, and moment arm on the moment-angle relationship of musculotendon actuators at the hip, knee, and ankle. *J. Biomechanics.*, **23**: 157-169 (1990).

[19] Kane, T.R. and Levinson, D.A. *Dynamics Online: Theory and Implementation with* AUTOLEV. Online Dynamics, Inc. Sunnyvale, CA. (1996).

[20] King, A.I. A review of biomechanical models *J. Biomech. Engrg.*, **106**: 97-104 (1984).

[21] Lanyon, L.E., Hampson, W.G.J., Goodship, A.E., and Shah, J.S. Bone deformation recorded in vivo from strain gauges attached to the human tibia shaft. *Acta Ortho. Scand.*, **46:** 256-268 (1974).

[22] Lockwood, P. A three dimensional model of dynamic human eye movement. *Ph.D. Dissertation*, Department of Mathematics and Statistics, Texas Tech University (1998).

[23] McMahon, T.A. *Muscles, Reflexes, and Locomotion*, Princeton University Press, Princeton, New Jersey (1984).

[24] Patriarco, A.G., Mann, R.W., Simon, S.R., and Mansour, J.M., An evaluation of the approaches of optimization models in the prediction of muscle forces during human gait. *J. Biomechanics.*, **14**: 513-525 (1981).

[25] Robinson, D.A., The mechanics of human saccadic eye movement, *J. of Physiol.*, **174**:245-264, (1964).

[26] Seireg, A., and Arvikar, R.J. The prediction of muscular load sharing anf joint forces in the lower extremities during walking. *J. Biomechanics.*, **8**: 89-102 (1975).

[27] Toridis, T. Stress analysis of the femur. *J. Biomechanics.*, **2**: 163-174 (1964).

[28] Winter, D.A. *The Biomechanics and Motor Control of Human Gait.* University of Waterloo Press, Waterloo, Ontario, Canada (1987).

[29] Yamaguchi, G.T., and Zajac, F.E. Restoring unassisted natural gait to paraplegics via functional neuromuscular stimulation: A computer simulation study. *IEEE Trans. Biomed. Engrg.,* **37**: 886-902 (1990).

[30] Yamaguchi, G.T. Feasibility and Conceptual design of functional neuromuscular stimulation systems for the restoration of natural gait to paraplegics based on dynamic musculoskeletal models. *Ph.D. Thesis,* Department of Mechanical Engineering, Stanford University, Stanford, CA Aug. (1989).

[31] Zajac, F.E. Muscle and tendon: Properties, models, scaling, and application to biomechanics and motor control. *In CRC Critical Reviews in Biomechanical Engineering.* **17**: 359-410 (1989).

Department of Mathematics, Texas Tech University, Lubbock, Tx 79409

Department of Mathematics, Texas Tech University, Lubbock, Tx 79409